CHAPTER 4

DISCUSSION OF RESULTS

4.1 Introduction

In solid state reactions, the reactants react in the solid state to yield newly formed products. At standard temperature and pressure, these reactions are usually extremely slow and high temperatures are often required for these reactions to occur at an appreciable rate. Only at sufficiently high temperatures, certain ions obtain the required thermal energy to enable them to move out of their normal lattice sites and diffuse through the crystals to form new products *[2]*.

The first stage in a solid state reaction involves the formation of product nuclei where the reactants are in close contact with each other *[2]*. The formation of product nuclei is often difficult when there are considerable differences in structure between the reactants and the products. In such cases, large amounts of structural reorganization are often involved in forming the products; bonds must be

broken and formed and atoms must migrate over sometimes considerable distances (on atomic scale) *[2]*.

In the preparative procedures followed in this study, the rates of reactions between the reactants in the raw mixes (i.e. barium oxide, silica, alumina and ferric oxide) were probably mainly influenced by the following factors *[2, 4]*:

1) the areas of contact between the reacting solids;
2) the rates of nucleation of the intermediate or product phases;
3) the rates of diffusion of ions through the various phases.

As mentioned in Chapter 3, the nature of the bonding forces present in a solid substance determines the spatial arrangements that the species will settle into, but these arrangements will always represent a configuration with minimum electrostatic interactions or lattice energy *[26]*. The characteristics of solid materials such as the silicates and metal oxides were of particular importance in this study. These materials are composed of atoms that display both ionic and covalent character in their bonding and usually form chains that extend through the entire crystal *[9, 26]*. It is therefore common to find a variety of stable crystalline forms in such solids.

These factors probably all contributed to the wide variety of crystalline phases that were detected in the different samples prepared during this study with change in heating temperature and heating time. Only some of the binary samples had relatively simple phase compositions. The crystalline phases identified in the quaternary samples with change in heating temperature and heating time are summarized in Table 4.1[1]. In this chapter, the formation and properties of the detected phases will be discussed. Any trends observed in the formation of these phases will also be discussed.

[1] The cement chemist's notation as discussed in Chapter 1 was used to denote the different phases in Table 4.1.

Table 4.1: Summary of the phases detected in the quaternary samples with M_A = 1.5, M_S = 2.3 and different BSF values.

Temp. (°C)	Time (min)	Phases Detected				
		BSF = 86 %	BSF = 90 %	BSF = 94 %	BSF = 98 %	BSF = 102 %
900	60	$B\bar{C}$, B_2S, BS, B_3A	$B\bar{C}$, B_2S, BS, B_3A	$B\bar{C}$, B_2S, BS, B_3A	$B\bar{C}$, B_2S, BS, B_3A	$B\bar{C}$, B_2S, BS, B_3A
1000	15	$B\bar{C}$, B_2S, BS, BA, B_3A	$B\bar{C}$, B_2S, BS, BA, B_3A	$B\bar{C}$, B_2S, BS, BA, B_3A	$B\bar{C}$, B_2S, BS, BA, B_3A	$B\bar{C}$, B_2S, BS, B_3A
1000	30	$B\bar{C}$, B_2S, BS, BA, B_3A, BH_4	$B\bar{C}$, B_2S, BS, BA, B_3A, BH	$B\bar{C}$, B_2S, BS, BA, B_3A	$B\bar{C}$, B_2S, BS, BA, B_3A	$B\bar{C}$, B_2S, B_3A
1000	60	$B\bar{C}$, B_2S, BS, BA, B_3A, BH	$B\bar{C}$, B_2S, BS, B_3A	$B\bar{C}$, B_2S, BS, BA, B_3A, BH	$B\bar{C}$, B_2S, BS, BA, B_3A	$B\bar{C}$, B_2S, B_3A
1000	120	$B\bar{C}$, B_2S, BS, BA, B_3A, BH	$B\bar{C}$, B_2S, BS, B_3A	$B\bar{C}$, B_2S, BS, B_3A, BH	$B\bar{C}$, B_2S, BS, B_3A	$B\bar{C}$, B_2S, B_3A
1100	15	$B\bar{C}$, B_2S, BS, BA, B_3A, BH	$B\bar{C}$, B_2S, BS, BAS, BA, B_3A	$B\bar{C}$, B_2S, BS, BAS, BA, B_3A	$B\bar{C}$, B_2S, BS, BA, B_3A	$B\bar{C}$, B_2S, BS, BA, B_3A
1100	30	$B\bar{C}$, B_2S, BS, B_3A, BH	$B\bar{C}$, B_2S, BS, BAS, BA, B_3A	$B\bar{C}$, B_2S, BS, BAS, B_3A, BH	$B\bar{C}$, B_2S, BS, BAS, B_3A	$B\bar{C}$, B_2S, BS, BA, B_3A
1100	60	$B\bar{C}$, B_2S, BS, B_3A, BH_2, BH_9	$B\bar{C}$, B_2S, BS, BAS, B_3A, BH	$B\bar{C}$, B_2S, BS, BAS, B_3A	$B\bar{C}$, B_2S, BS, BAS, B_3A	$B\bar{C}$, B_2S, BA, B_3A
1100	120	$B\bar{C}$, B_2S, BS, BAS, B_3A, BH_2, BH_9	$B\bar{C}$, B_2S, BAS, B_3A, BH_2, BH_9	$B\bar{C}$, B_2S, BS, BAS, B_3A, BH_2, BH_9	$B\bar{C}$, B_2S, BS, BAS, B_3A, BH_2	$B\bar{C}$, B_2S, BAS, B_3A, BH_2
1200	15	$B\bar{C}$, B_2S, BS, BAS, BA, B_3A, BH, BH_9	$B\bar{C}$, B_2S, BS, BA, B_3A, BH	$B\bar{C}$, B_2S, BS, BA, B_3A	$B\bar{C}$, B_2S, BS, BA, B_3A	$B\bar{C}$, B_2S, BS, BAS, BA, B_3A
1200	30	$B\bar{C}$, B_2S, BS, BAS, BA, B_3A, BH_4, BH_9	$B\bar{C}$, B_2S, BS, BA, B_3A, BH_9	$B\bar{C}$, B_2S, BS, BA, B_3A, BH	$B\bar{C}$, B_2S, BS, BAS, BA, B_3A	$B\bar{C}$, B_2S, BS, BAS, BA, B_3A
1200	60	$B\bar{C}$, B_2S, BS, BAS, BA, B_3A, BH_4, BH_9	$B\bar{C}$, B_2S, BS, BA, B_3A, BH_4, BH_9	$B\bar{C}$, B_2S, BS, BAS, B_3A, BH, BH_9	$B\bar{C}$, B_2S, BS, BAS, B_3A, BH_2	$B\bar{C}$, B_2S, BS, BAS, BA, B_3A, BH_2
1200	120	$B\bar{C}$, B_2S, BS, BAS, B_3A, BH_9	$B\bar{C}$, B_2S, BS, BAS, B_3A, BH_9	$B\bar{C}$, B_2S, BAS, B_3A, BH_4, BH_9	$B\bar{C}$, B_2S, B_3A, BH_2, BH_4	$B\bar{C}$, B_2S, BS, BAS, B_3A, BH_2

Table 4.1: (Continued)

Temp. (°C)	Time (min)	Phases Detected				
		BSF = 86 %	**BSF = 90 %**	**BSF = 94 %**	**BSF = 98 %**	**BSF = 102 %**
1300	15	$B\bar{C}$, B_2S, BS, BA, B_3A, BH_2, BH_4, BH_9	$B\bar{C}$, B_2S, BS, BA, B_3A, BH_2, BH_4, BH_9	$B\bar{C}$, B_2S, BS, BAS, BA, B_3A, BH_2	$B\bar{C}$, B_2S, BS	$B\bar{C}$, B_2S, BS, BAS, BA, B_3A
1300	30	$B\bar{C}$, B_2S, BS, BAS, B_3A, BH_4, BH_9	$B\bar{C}$, B_2S, BS, BAS, BA, B_3A, BH_4, BH_9	$B\bar{C}$, B_2S, BS, BAS, BH_9	$B\bar{C}$, B_2S, BS, BH_2, BH_4	$B\bar{C}$, B_2S, BS, BAS, BA, B_3A
1300	60	B_2S, $B\bar{C}$, BS, BAS, B_3A, BH, BH_9	$B\bar{C}$, B_2S, BS, BAS, BA, B_3A, BH, BH_2, BH_4	$B\bar{C}$, B_2S, BS, BAS, BH, BH_2, BH_9	$B\bar{C}$, B_2S, BAS, BH_2	$B\bar{C}$, B_2S, BAS, BA, B_3A
1300	120	$B\bar{C}$, B_2S, BAS, BH, BH_9	$B\bar{C}$, B_2S, BS, BAS, B_3A, BH, BH_4	$B\bar{C}$, B_2S, BS, BAS, BH_9	$B\bar{C}$, B_2S, BAS, BH_2	$B\bar{C}$, B_2S, BAS, B_3A, BH_2
1400	15	B_2S, $B\bar{C}$, BS, BAS, BA, B_3A, BH, BH_4, BH_9	B_2S, $B\bar{C}$, BS, BAS, BA, B_3A, BH, BH_9	$B\bar{C}$, B_2S, BS, BA, B_3A, BH_2	$B\bar{C}$, B_2S, BS, BH_2	$B\bar{C}$, B_2S, BS, BAS, B_3A
1400	30	$B\bar{C}$, B_2S, BS, BAS, B_3A, BH_2, BH_9	B_2S, $B\bar{C}$, BAS, BA, BH, BH_2	$B\bar{C}$, B_2S, BA, B_3A, BH_2, BH_9	$B\bar{C}$, B_2S, BS, BH_2	$B\bar{C}$, B_2S, BS, BAS, B_3A
1400	60	$B\bar{C}$, B_2S, BAS, BH, BH_2, BH_9	B_2S, $B\bar{C}$, BAS, BH_2, BH_9	$B\bar{C}$, B_2S, B_3A, BH_2, BH_9	$B\bar{C}$, B_2S, BH_2, BH_9	$B\bar{C}$, B_2S, BS, BAS, B_3A
1400	120	$B\bar{C}$, B_2S, BH, BH_4, BH_9	B_2S, $B\bar{C}$, BAS, BH, BH_2, BH_9	$B\bar{C}$, B_2S, BH_2, BH_9	$B\bar{C}$, B_2S, BH_2	$B\bar{C}$, B_2S, BS, BAS, B_3A, BH_2

4.2 Barium Carbonate and Barium Hydroxide Phases

4.2.1 Thermal Decomposition of Barium Carbonate

Upon heating of barium carbonate in air at standard pressure, two phase transformations of barium carbonate occur, as depicted in Equation 4a *[17, 28]*. Both of these phase transformations are endothermic *[28]*. The first transformation, occurring at approximately 811 °C, is the conversion of orthorhombic to hexagonal barium carbonate and the second transformation, occurring at approximately 982 °C, is the conversion of hexagonal to cubic barium carbonate *[28]*.

$$BaCO_3(\gamma) \xrightarrow{811^\circ C} BaCO_3(\beta) \xrightarrow{982^\circ C} BaCO_3(\alpha) \qquad (4a)$$

Heating at temperatures higher than 1360 °C results in the decarbonation of barium carbonate according to Equation 4b *[17]*. The activation energy for this decarbonation reaction is 305 (±14) kJ.mol^{-1} *[28]*. (The activation energy for the decarbonation of pure calcium carbonate is 167 kJ.mol^{-1} *[6]*).

$$BaCO_3(s) \longrightarrow BaO(s) + CO_2(g) \qquad (4b)$$

Arvanitidis et al. *[28]* studied this decarbonation reaction in a spherical compact (nodule) consisting of only barium carbonate. According to these authors, the decomposition reaction is topochemical starting at the surface of the nodule. Therefore, since the molar volume of barium oxide is considerably lower than that of barium carbonate *[17]* and since carbon dioxide is evolved during the decomposition of barium carbonate, the unreacted barium carbonate core will eventually be covered by a porous barium oxide layer when heated to a sufficiently high temperature *[5, 28]*. It is possible that this oxide layer will crack and even break apart as the decarbonation reaction continues *[28]*.

For a nodule consisting of pure barium carbonate, the rate of the decomposition reaction is likely to be controlled by one or more of the following steps *[5, 28]*.

1) the decomposition reaction at the surface of the barium carbonate core (Equation 4b);
2) the transport of carbon dioxide from the $BaCO_3$-BaO interface through the oxide layer out to the surrounding atmosphere;
3) the transport of carbon dioxide away from the nodule;
4) transport of heat from the surrounding to the $BaCO_3$-BaO interface through the oxide layer.

Furthermore, since an eutectic reaction between barium carbonate and barium oxide seems to occur at 33 mole percent barium oxide *[28]*, it appears likely that liquid formation will occur at some stage during heating of a nodule containing barium carbonate. If liquid formation occurs at the $BaCO_3$-BaO interface, the transport of carbon dioxide through the liquid layer out to the surrounding oxide layer will also have an effect on the rate of the decomposition reaction.

In the case of calcium carbonate, it is known that the decarbonation reaction starts at a much lower temperature when silica, alumina and ferric oxide are present *[4, 5]*. Usually, much carbon dioxide is evolved before any free (uncombined) calcium oxide is detected, mainly due to the early formation of dicalcium silicate *[5]*. In Chapter 2 (Figures 2.1 to 2.6), it was seen that in the presence of silica, alumina and ferric oxide, the decarbonation of barium carbonate also commenced at a considerably lower temperature (approximately 550 to 600 °C). This indicates that the initial reactions between barium carbonate and the other oxides in the mixtures were possibly analogous to that of calcium carbonate.

It was also seen in Chapter 2 that the decomposition temperature of barium carbonate in the quaternary samples varied with BSF value of the mixture. It therefore appears that the quantity of silica, alumina and ferric oxide in the mixture played a role in the decarbonation of barium carbonate: for the range of BSF values studied, it seems that the lower the BSF value of the mixture (i.e. a higher oxides content), the lower the temperature at which the decomposition commenced. However, for all BSF values, the temperature at which the rate of decarbonation

was highest remained the same at approximately 1130 °C (for pure barium carbonate, this temperature was 1186 °C).

In addition, it can be seen in Figures 2.1 to 2.6 that in the presence of silica, alumina and ferric oxide, the decomposition occurred in two steps as compared to a single step in the case of pure barium carbonate. The second step commenced at approximately 800 °C in all samples and continued until completion of the decomposition at 1150 to 1190 °C, depending on the BSF value of the mix. At 800 °C, approximately 15 % of the barium carbonate in the samples was decarbonized. If the reactions of barium carbonate with the oxides are analogous to that of calcium carbonate up to 800 °C, very little barium oxide is expected to have been present in the samples at this stage. Hence, it is unlikely that a eutectic mixture between barium oxide and barium carbonate had been reached at this stage. At higher temperatures, however, the rate of decarbonation increased and it is possible that the uncombined barium oxide content in the samples increased accordingly. The formation of a eutectic mixture between barium oxide and barium carbonate therefore became more likely. Such liquid formation would probably have made decarbonation of the barium carbonate in the core of the nodule more difficult, but, on the other hand, it would have facilitated the solid state reaction between barium oxide and the other oxides in the sample mixtures.

X-ray diffraction analysis of the prepared samples showed that barium carbonate was present in all the quaternary samples, indicating that equilibrium conditions probably had not yet been reached and/or that an excess of barium carbonate was initially present in these samples. In samples with the same BSF value, the amount of the carbonate present appeared to decrease with an increase in heating temperature and heating time. Heating at the higher temperatures probably increased the rates at which barium oxide reacted with the other oxides in the mixtures, so that less uncombined barium oxide was present at the higher temperatures. Heating for longer at a specific temperature allowed more time for the barium oxide to react with the other oxides, also resulting in less uncombined barium oxide in such samples.

At the higher heating temperatures, the carbonate content of the samples appeared to decrease with a decrease in BSF value. This was probably due to the samples with the higher BSF values having a bigger "excess" of barium oxide at equilibrium. The binary and ternary samples, in general, did not contain any barium carbonate and as the diffractograms of these samples did not change further when heated for longer, it appears that equilibrium conditions had been attained in these samples. Only the binary sample with raw mix composition of $BaCO_3$:Fe_2O_3 = 2:1, contained a very small fraction of barium carbonate.

4.2.2 Reactions of Barium Oxide in Air

In the preceding section, it was seen that barium oxide is formed during the thermal decomposition of barium carbonate. Some uncombined barium oxide was therefore expected to be present in at least some of the samples, in particular those with the highest BSF values. However, no barium oxide was detected by X-ray diffraction analysis in any of the samples prepared during this study. Instead, most samples contained some barium hydroxide and/or barium carbonate.

Barium oxide is known to be extremely reactive in air and readily reacts with moisture and carbon dioxide to form barium hydroxide and barium carbonate *[29]*. The heat of formation of barium hydroxide from barium oxide and water is 102 $kJ.mol^{-1}$ and that of barium carbonate from barium oxide and carbon dioxide is 264 $kJ.mol^{-1}$ *[29]*.

With the equipment available for this study, it was not possible to protect the prepared samples from exposure to moisture and carbon dioxide under all circumstances: all samples were exposed to air during cooling of the clinker, grinding of the samples and during X-ray diffraction analysis. These exposures to air probably all contributed to the initially uncombined barium oxide in the burned samples being rapidly converted to the more stable barium hydroxide and/or barium carbonate forms. This observation is in agreement with that of other authors who studied the solid state reaction of barium carbonate with amorphous silica and also did not detect free barium oxide in any of their samples *[30]*.

In Figure 4.1, the diffractogram of a "fresh" sample is compared to that of the same sample after a longer exposure to air. It can clearly be seen that, on exposure to air, the quantity of barium hydroxide monohydrate decreased with a corresponding increase in the quantity of barium carbonate in the sample. It therefore appears that, on exposure to air, barium oxide was first converted to the hydroxide form(s) and then to the carbonate form, as described by Equation 4c. The other phases present in the sample, such as dibarium silicate, appeared to be unaffected for the duration of exposure to air.

$$BaCO_3(s) \xrightarrow{heat} BaO(s) + CO_2(g) \xrightarrow{air} Ba(OH)_2.xH_2O(s) \xrightarrow{air} BaCO_3(s) \quad (4c)$$

where x = 0, 1, 3 or 8.

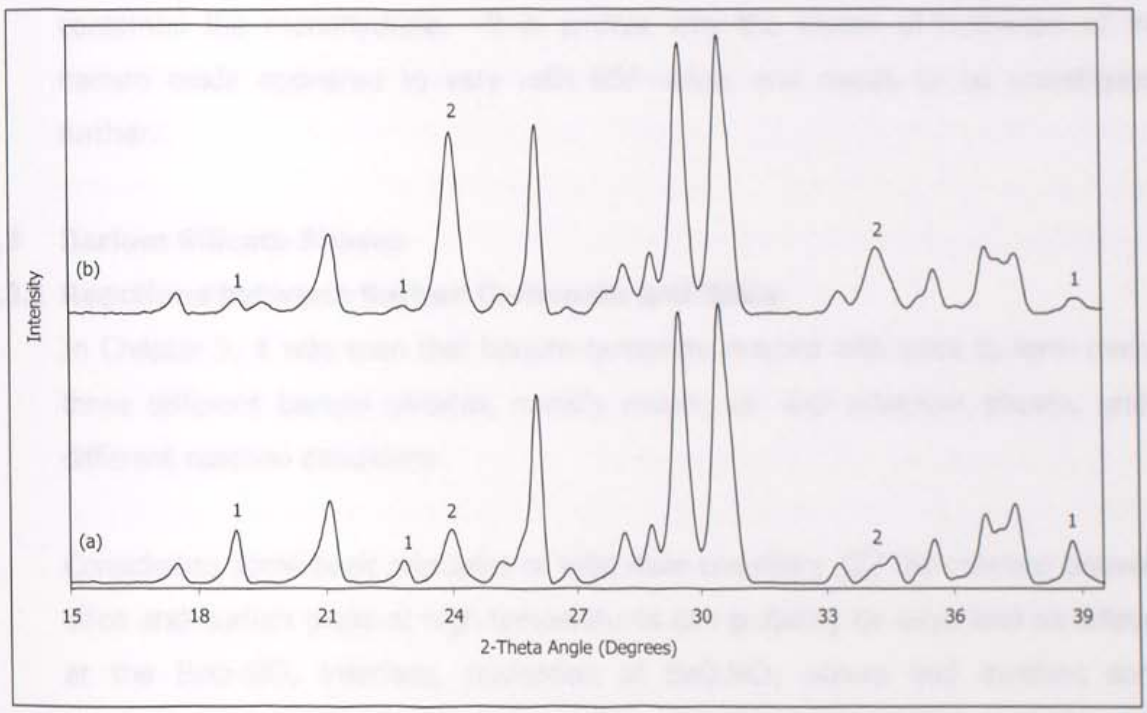

Figure 4.1: Comparison of diffractograms of (a) a fresh sample and (b) after the same sample was exposed to air. Peaks mainly due to barium hydroxide monohydrate are indicated by 1; peaks mainly due to barium carbonate are indicated by 2.

It appears that the only feasible way for the different barium hydroxides to form in the samples must have been through the hydration of barium oxide (Equation 4c).

If this was the case, then the presence of the barium hydroxides in most of the quaternary samples confirms that some uncombined barium oxide has been present in the samples initially.

From Table 4.1, it can be seen that, in general, for samples with a specific BSF value, a bigger variety of barium hydroxides was detected as the heating temperature and heating time were increased. At a specific heating temperature and time, more hydroxides were detected as the BSF value of the mix decreased. Furthermore, the extent of hydration of the barium oxide seemed to increase with a decrease in BSF value: most samples with BSF = 86 % contained some barium hydroxide octahydrate, whereas less of the samples with intermediate BSF values contained the octahydrate and none of the samples with BSF = 102 % contained the octahydrate. Instead, most of the samples with the higher BSF values contained the monohydrate. It is unclear why the extent of hydration of the barium oxide appeared to vary with BSF value, and needs to be investigated further.

4.3 Barium Silicate Phases

4.3.1 Reactions between Barium Carbonate and Silica

In Chapter 3, it was seen that barium carbonate reacted with silica to form mainly three different barium silicates, namely mono-, di- and tribarium silicate, under different reaction conditions.

Considering some basic principles of solid state chemistry *[2]*, the reaction between silica and barium oxide at high temperatures can probably be described as follows: at the BaO-SiO_2 interface, nucleation of $BaO.SiO_2$ occurs and involves some reorganization of the oxide ions at the site of the potential nucleus together with the possible interchange of Si^{4+} and Ba^{2+} ions across the interface between the SiO_2 and BaO.

The second stage involves the growth of a product layer, which may have been an even more difficult process than nucleation *[2]*. In order for the reaction to

continue and the $BaO.SiO_2$ layer to grow thicker, Ba^{2+} ions must diffuse through the existing $BaO.SiO_2$ product layer to the new reaction interfaces. It is possible that counter-diffusion of Si^{4+} ions also occurs through the product layer. At this stage there are two reaction interfaces: that between SiO_2 and $BaO.SiO_2$ and that between $BaO.SiO_2$ and BaO. Further reaction takes place only slowly and at a decreasing rate as the product layer grows thicker. In order to maintain charge balance, for every Si^{4+} ion that diffuses to the $BaO.SiO_2$-BaO interface, two Ba^{2+} ions must diffuse to the SiO_2-$BaO.SiO_2$ interface. (However, it must be noted that in cases where the reaction between CaO and SiO_2 were studied, no conclusive evidence was found for the counter-diffusion of Si^{4+} ions *[8]*). The rate of product formation at the two interfaces would therefore be different, resulting in products with variable composition. At the $BaO.SiO_2$-BaO interface, the reactions proceed to yield barium-rich phases such as $2BaO.SiO_2$ and, under certain conditions, even $3BaO.SiO_2$. Conversely, at the SiO_2-$BaO.SiO_2$ interface, barium-poor phases such as $BaO.2SiO_2$ probably forms, although such phases were not detected in any of the prepared samples. The quantities of barium hydroxide and barium carbonate present in the quaternary samples suggest that an "excess" of barium carbonate was present in the raw mixes, which, seemingly, made conditions unfavourable for the existence of the barium-poor phases such as $BaO.2SiO_2$.

Yamaguchi et al. *[30]* studied the solid state reaction between barium carbonate and amorphous silica, with Ba:Si = 2:1, in air in the temperature range 850 to 950 °C by means of thermogravimetry and X-ray diffraction analysis. These authors proposed that the overall reaction between barium carbonate and silica basically consists of the two consecutive reactions given by Equations 4d and 4e:

$$2BaCO_3(s) + SiO_2(s) \longrightarrow BaSiO_3(s) + BaCO_3(s) + CO_2(g) \quad (4d)$$

$$BaSiO_3(s) + BaCO_3(s) \longrightarrow Ba_2SiO_4(s) + CO_2(g) \quad (4e)$$

These two reactions are not completely sequential, with one overlapping the other *[30]*. The extent of overlap depends on the particle size ratio of $BaCO_3$ to SiO_2.

When the particle size ratio is large (for example 25:1), the biggest overlap occurs: a relatively small fraction of the silica is in direct contact with the barium carbonate particles, so that newly formed $BaO.SiO_2$ starts reacting with $BaCO_3$ to form $2BaO.SiO_2$ before all SiO_2 is consumed. On the other hand, when the particle size ratio is small (for example 5:1), all the silica is quickly consumed through the rapid formation of $BaO.SiO_2$. The $BaO.SiO_2$ then reacts in a second step with $BaCO_3$ to form $2BaO.SiO_2$, so that minimal overlap occurs.

Similarly to the solid state reaction between calcium carbonate and silica where the Ca^{2+} ions migrate easier than the Si^{4+} ions *[4, 8]*, Yamaguchi et al. suggested that the Ba^{2+} ions probably also migrate easier than the Si^{4+} ions *[30]*. In the reaction between BaO and SiO_2, the ratio of $BaO.SiO_2$ to $2BaO.SiO_2$ at any stage appears to depend on

1) the rate of diffusion of barium ions through the product phases, i.e. $BaO.SiO_2$ and $2BaO.SiO_2$, and

2) the rates of formation of $BaO.SiO_2$ and $2BaO.SiO_2$ at the phase boundaries *[30]*.

During their studies, Yamaguchi et al. detected only the mono- and dibarium silicates by means of X-ray diffraction *[30]*. No tribarium silicate or other barium silicates were detected. In this regard, it is also notable that other authors prepared single crystals of dibarium silicate by solid state reaction of an excess of BaO (molar ratio $BaO:SiO_2 = 88:12$) heated for 45 hours at a temperature of 1300 °C *[31]*. Furthermore, Boikova et al. doubted the existence of tribarium silicate *[19]*. Contrary to all these findings, it was seen in Chapter 3 that the samples prepared from the binary mixtures with $BaO:SiO_2$ in 2:1 and 3:1 molar ratios, contained mixtures of dibarium silicate and tribarium silicate, while no monobarium silicate was detected in these two samples. The discrepancies between the results of the above-mentioned authors and that obtained during this study are possibly due to the higher heating temperature and the longer heating times employed during the preparations in this study. The longer heating times (480 to 550 hours) at a temperature of 1400 °C probably allowed all monobarium silicate to be converted to dibarium silicate and probably also facilitated the

formation of tribarium silicate. This would also explain why tribarium silicate was not detected in any of the quaternary samples, which were heated for a maximum of only two hours at a maximum temperature of 1400 °C.

Considering Table 4.1, it can be seen that, in general, the quaternary samples with BSF values from 86 to 98 % contained monobarium silicate (BS) up to a heating time of 30 to 60 minutes at a heating temperature of 1300 °C, or 15 to 30 minutes at a temperature of 1400 °C. Dibarium silicate was detected in all quaternary samples. It therefore appears that heating for 60 minutes at 1300 °C or for 30 minutes at 1400 °C was sufficient to convert all of the monobarium silicate to dibarium silicate in these samples. However, the samples with a BSF value of 102 % contained monobarium silicate irregularly up to a heating time of 120 minutes at 1400 °C.

4.4 Barium Aluminium Silicate Phase

As can be seen in Table 4.1, hexagonal barium aluminium silicate (BAS) was present in most of the quaternary samples that were prepared at heating temperatures of 1100 °C and higher. No barium aluminium silicate was detected in samples prepared at heating temperatures below 1100 °C. It should be noted, however, that in all cases where barium aluminium silicate was detected, only very low peak intensities were observed for this phase in the respective diffractograms, probably as a result of relatively small quantities of this phase being present. These low peak intensities, together with the large number of peaks from the other phases present, made it very difficult to unambiguously assign the various peaks to the minor phases.

From the results in Table 4.1, it appears that under the chosen reaction conditions the formation of barium aluminium silicate has been unaffected by the BSF value of the samples or heating time and apparently only depended on the heating temperature.

The calcium analogue of monobarium aluminium silicate is not known to form in

ordinary Portland cement *[4, 5]*. In the $CaO-Al_2O_3-SiO_2$ system, mainly two calcium aluminosilicates are known to form, namely C_2AS and CAS_2 *[5]*. Of these, only C_2AS is of some relevance to cement chemistry *[5]*.

4.5 Barium Aluminate Phases

In Chapter 3, it was seen that barium oxide reacted with aluminium oxide to form monobarium aluminate (BA) and/or tribarium aluminate (B_3A). Similarly to monobarium aluminium silicate, these two phases were present in the quaternary samples as minor phases only, so that their low peak intensities, together with the large number of peaks from the other phases present, made it very difficult to unambiguously assign the various peaks in the different diffractograms to these two phases.

In general, monobarium aluminate was present up to a heating time of 30 minutes at all heating temperatures from 1000 to 1400 °C, in samples with BSF values from 86 to 94 %. In samples with BSF values of 98 and 102 %, monobarium aluminate was present up to heating temperatures of only 1200 and 1300 °C, respectively. Tribarium aluminate phase was detected in most of the quaternary samples and no specific trend was observed for this phase.

In Chapter 3, it was seen that monobarium aluminate is the equilibrium phase formed in the binary system with $BaO:Al_2O_3 = 1:1$. This is in agreement with the findings of other authors who studied the equimolar $BaO-Al_2O_3$ system at a heating temperature of 1450 °C *[32]*. Furthermore, it was seen in Chapter 3 that tribarium aluminate is the only phase formed in the binary system with $BaO:Al_2O_3 = 3:1$ at 1400 °C.

In the ternary system with $BaO:Al_2O_3:Fe_2O_3 = 4:1:1$ heated at 1100 °C for 500 hours, monobarium aluminate was the only aluminate phase detected, in addition to the various barium-rich ferrite phases. Since tribarium aluminate was expected to form if sufficient barium oxide was available, it appears that in the ternary system $BaO-Al_2O_3-Fe_2O_3$, barium oxide was consumed by ferric oxide in

preference to aluminium oxide, under the chosen reaction conditions. Consequently there was only sufficient barium oxide available in this ternary sample to form the barium-poor monobarium aluminate phase.

The CaO-Al_2O_3 system contains the stable phases C_3A, CA, $C_{12}A_7$, CA_2 and CA_6 *[4]*. Pure C_3A does not exhibit polymorphism. It is cubic and built from Ca^{2+} ions and rings of six AlO_4 tetrahedra, of formula $Al_6O_{18}^{18-}$ *[5]*. Substantial proportions of the Al^{3+} in these structures can be replaced by other ions, of which Fe^{3+} (3 to 4 % substitution, expressed as Fe_2O_3) and Si^{4+} (2 % substitution, expressed as SiO_2) are the most important *[5]*. In the CaO-SiO_2 system, a phase of approximate composition $C_{12}A_7$ readily forms *[5]*, but no evidence for the barium analogue was found during this study.

4.6 Barium Ferrite Phases

It was seen in Chapter 3 that the binary system with BaO:Fe_2O_3 = 2:1 contained mainly dibarium ferrite (B_2F) and small quantities of tribarium ferrite (B_3F) and barium diferrite (BF_2) after heating for 16 hours at 1000 °C. The dibarium ferrite and barium diferrite phases are analogous to the calcium ferrite phases formed in the system CaO-Fe_2O_3; in the binary system CaO-Fe_2O_3, three stable phases are formed, viz. C_2F, CF and CF_2 *[5]*.

As discussed in the preceding section, the ternary sample mixture that had a molar ratio of BaO:Al_2O_3:Fe_2O_3 = 4:1:1, yielded a mixture of phases consisting of monobarium aluminate, dibarium ferrite and tribarium ferrite. The broad band observed in the region of 15 °2θ in the diffractogram of this sample indicates that some amorphous material was probably also present. Considering that the BaO:Al_2O_3 and BaO:Fe_2O_3 molar ratios were equal in this ternary sample mixture, and that only the barium-poor aluminate phase (BA) formed compared to the barium-rich ferrite phases that formed, it appears that barium oxide was preferentially consumed by ferric oxide.

No barium ferrite phases were detected in any of the diffractograms of the quaternary samples prepared during this study. It is possible that the quantities of the ferrite phases that formed were lower than the detection limits of the X-ray diffractometer. It is also possible that the ferrite phases that formed were amorphous in nature and would therefore not have been detected by X-ray diffraction. A further possibility is that the ferric oxide was taken up as "impurities" by the other phases, forming solid solutions.

According to West *[2]*, a solid solution is basically a crystalline phase that can have variable composition. In a substitutional solid solution the atom or ion that is being introduced directly replaces an atom or ion of the same charge in the parent structure. In an interstitial solid solution the introduced atom or ion occupies a site that is normally empty on the crystal structure and no atoms or ions are left out.

For a simple substitutional solid solution to form, the following minimum requirements must be met:

1) the ions that are replacing each other must have the same charge (otherwise vacancies or interstices would be created) and

2) the ions must be similar in size (a difference of 15 % in the radii is the most that can be tolerated for a substitutional solid solution).

A larger cation would prefer octahedral coordination relative to tetrahedral coordination in a solid solution. In cases where the two ions are considerably different in size, the larger ion may be partially replaced by a smaller one, but it is more difficult to do the reverse and replace a small ion with a larger one *[2]*.

In Portland cement clinker, the dicalcium silicate phase contains approximately 4 to 6 % of substituent oxides, of which the major are usually alumina and ferric oxide. Tricalcium silicate can contain up to 1.0 % alumina or 1.1 % ferric oxide *[5]*. In these two calcium silicates, Fe^{3+} can partially substitute for Ca^{2+}, while Al^{3+} can substitute for Si^{4+} *[5]*. In the latter case, the Al^{3+} is usually occupied in tetrahedral

sites in the crystal structure *[5]*. Solid solution formation also occurs when Fe^{3+} is dissolved in C_3A, $C_{12}A_7$ and CA up to levels of 4.5 % (expressed as Fe_2O_3) *[4]*.

At ordinary pressures, in the absence of oxides other than calcium oxide, alumina and ferric oxide, the ferrite phase can be prepared with any composition in the solid solution series $Ca_2(Al_xFe_{1-x})_2O_5$, where $0 < x < 0.7$ *[4, 5]*. The composition C_4AF is only a point in this series, with $x = 0.5$.

4.7 Trends Observed in the Ratio of Dibarium Silicate to Barium Carbonate

It was seen in the preceding sections that dibarium silicate and barium carbonate were the two major phases detected by X-ray diffraction analysis in the quaternary samples. By comparing the X-ray diffraction reference patterns of these two major phases with those of the other constituents detected in the quaternary samples (see Chapter 3 and Appendix A), it can be seen that the peaks at $2\theta = 29.585°$ and $2\theta = 23.901°$ are almost solely due to the reflections of dibarium silicate and barium carbonate, respectively. If it is assumed that preferred orientation did not significantly affect these two peak intensities or that preferred orientation was similar in all the samples, then changes in the ratio of these two peak intensities for the different samples indicate changes in the (non-quantitative) ratio between the dibarium silicate and barium carbonate. However, it must be taken into account that, as already discussed earlier in this chapter, a variety of factors could have affected the extent of carbonation of barium oxide and/or hydroxide in the samples. Varying quantities of barium hydroxide and barium carbonate in the samples could also have influenced the intensity ratio of dibarium silicate to barium carbonate. In the following Sections 4.7.1 and 4.7.2, the trends observed in the ratio of the relevant peak intensities will be discussed with respect to heating time, heating temperature and BSF value.

4.7.1 Variation of B_2S:BC Ratio with Heating Time at Constant Temperature for Different BSF Values

Figures 4.2 to 4.6 show the variation with heating time of the intensity ratio of dibarium silicate to barium carbonate. In each figure the heating temperature was

held constant at either 1000, 1100, 1200, 1300 or 1400 °C, while the intensity ratios observed for each of the different BSF values are depicted. See Appendix B for the values of the $I(B_2S):I(BaCO_3)$ ratios as plotted in these figures.

Considering Figure 4.2, it can be seen that, in general, the intensity ratio of $B_2S:BaCO_3$ increased with heating time at 1000 °C. For some BSF values (90, 94 and 102 %) there was a slight decrease in the intensity ratio on moving from a heating time of 15 to 30 minutes. From a heating time of 30 minutes up to 120 minutes the ratio increased steadily for all samples. At 120 minutes, the samples with the lowest BSF values had the highest $I(B_2S):I(BaCO_3)$ ratio, probably indicating a smaller "excess" of barium carbonate in these samples.

At a heating temperature of 1100 °C (Figure 4.3), for most BSF values, the intensity ratio increased steadily from a heating time of 15 up to 120 minutes. However, for samples with BSF values of 86 and 98 %, the ratio increased with heating time, reaching a maximum at 60 minutes, after which it decreased again at 120 minutes.

From Figure 4.4, it can be seen that at a heating temperature of 1200 °C, the intensity ratio tended to increase with heating time for most BSF values. As previously, some samples did not follow this trend for all heating times. At a heating time of 120 minutes, the $I(B_2S):I(BaCO_3)$ ratio increased with a decrease in BSF value, probably indicating a smaller excess of barium carbonate as the BSF value of the samples decreased.

Considering Figure 4.5, it can be seen that for most BSF values the intensity ratio reached a maximum after heating for 30 to 60 minutes at 1300 °C. In addition, the intensity ratios for the samples heated at 1300 °C did not vary as much with heating time as those at the lower heating temperatures. The sample with a BSF value of 86 % had an abnormally high $I(B_2S):I(BaCO_3)$ ratio at a heating time of 60 minutes.

From Figure 4.6, it can be seen that at a heating temperature of 1400 °C, all BSF

values had a maximum intensity ratio at a heating time of only 15 minutes. The $I(B_2S):I(BaCO_3)$ ratio dropped drastically on moving from a heating time of 15 to 30 minutes, after which it remained relatively constant. The only exception to this trend was for those samples with a BSF value of 94 %, which reached a maximum ratio at a heating time of 60 minutes.

The intensity ratios as plotted in Figures 4.2 to 4.6 might be useful as a rough estimate to what extent the solid state reaction between barium carbonate and silica had proceeded to yield dibarium silicate. Considering Figures 4.2 to 4.6, it appears that the heating time was very important at heating temperatures of up to 1200 °C and long heating times would probably be required for the reaction to complete at these temperatures. At heating temperatures of 1300 °C and higher, the heating time became less important, so that shorter heating times would probably be required for the reaction to complete. Furthermore, the B_2S:BC ratio increased with a decrease in BSF value of the sample, indicating that a smaller excess of barium carbonate was present in these samples.

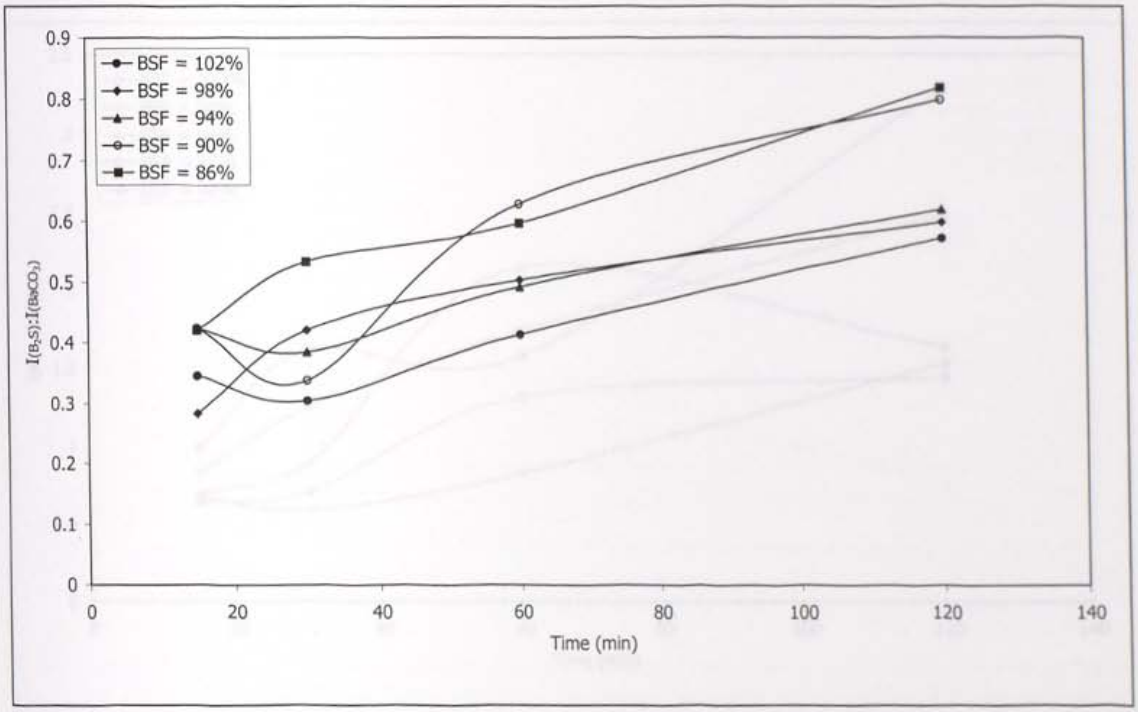

Figure 4.2: Intensity ratio of $B_2S(2\theta = 29.585°):BaCO_3(2\theta = 23.901°)$ with heating time at 1000 °C, for samples with different BSF values

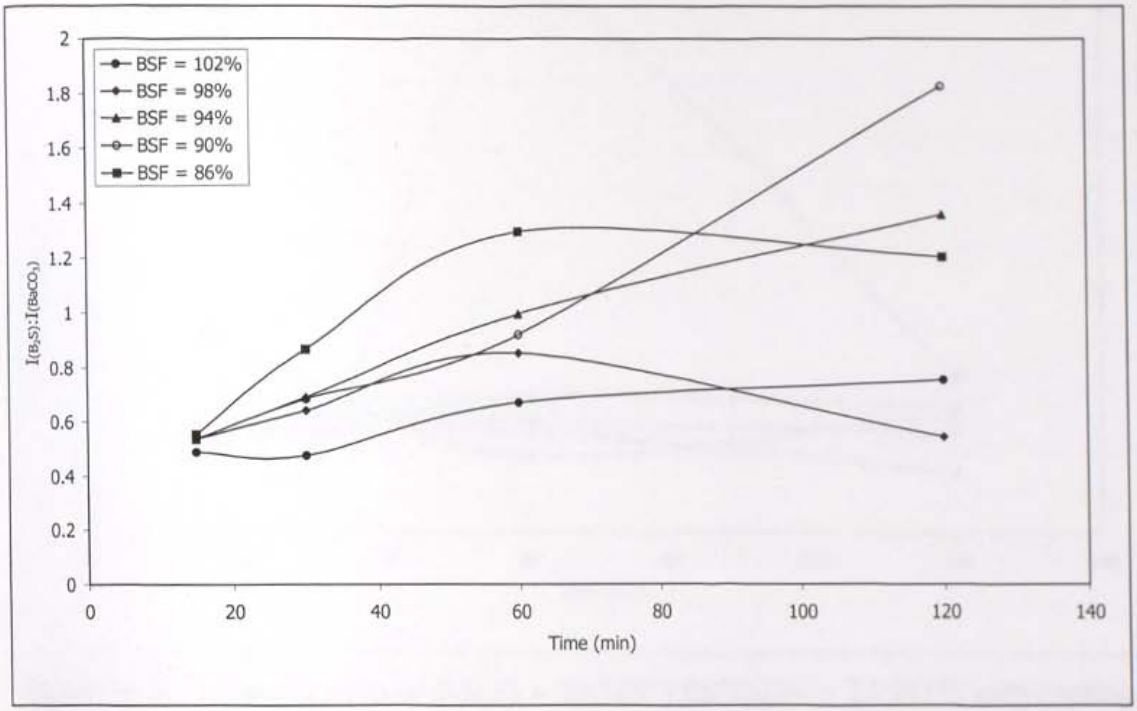

Figure 4.3: Intensity ratio of $B_2S(2\theta = 29.585°):BaCO_3(2\theta = 23.901°)$ with heating time at 1100 °C, for samples with different BSF values

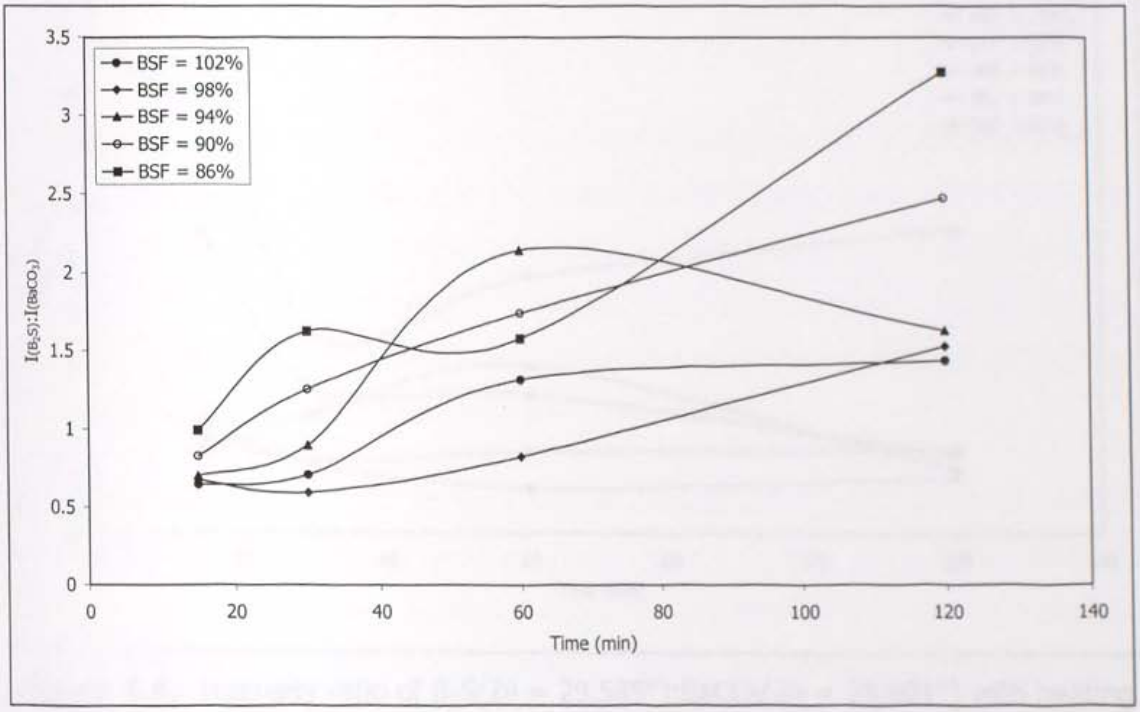

Figure 4.4: Intensity ratio of $B_2S(2\theta = 29.585°):BaCO_3(2\theta = 23.901°)$ with heating time at 1200 °C, for samples with different BSF values

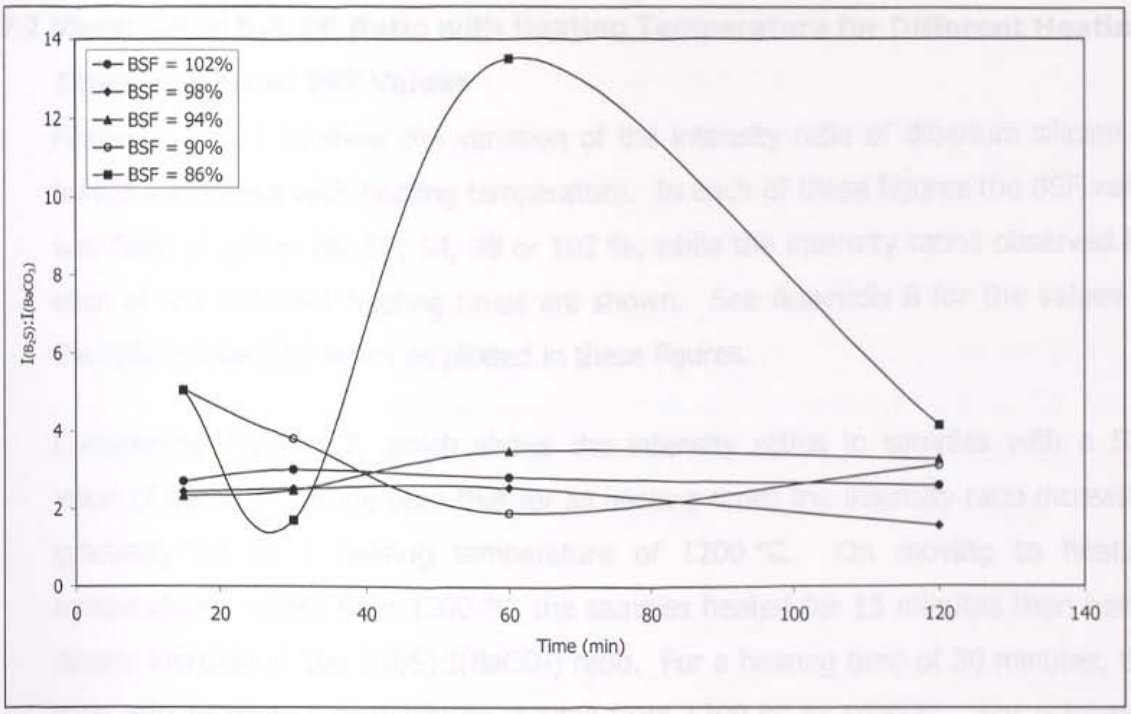

Figure 4.5: Intensity ratio of $B_2S(2\theta = 29.585°):BaCO_3(2\theta = 23.901°)$ with heating time at 1300 °C, for samples with different BSF values

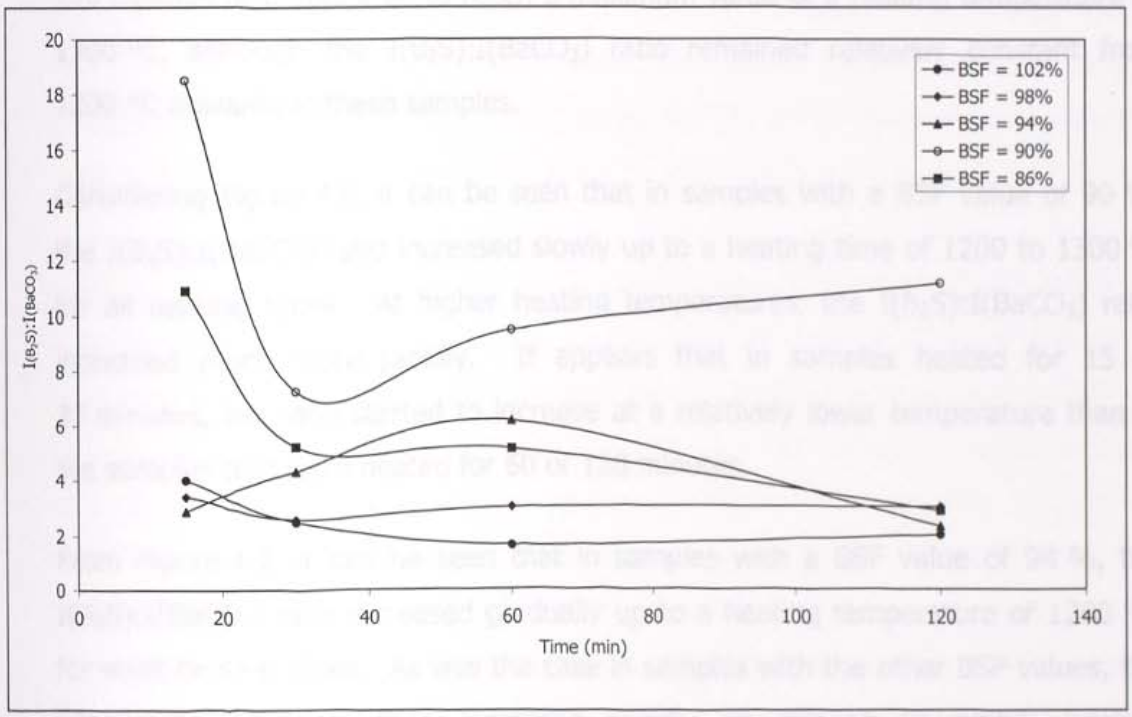

Figure 4.6: Intensity ratio of $B_2S(2\theta = 29.585°):BaCO_3(2\theta = 23.901°)$ with heating time at 1400 °C, for samples with different BSF values

4.7.2 Variation of B_2S:BC Ratio with Heating Temperature for Different Heating Times and Fixed BSF Values

Figures 4.7 to 4.11 show the variation of the intensity ratio of dibarium silicate to barium carbonate with heating temperature. In each of these figures the BSF value was fixed at either 86, 90, 94, 98 or 102 %, while the intensity ratios observed for each of the different heating times are shown. See Appendix B for the values of the $I(B_2S):I(BaCO_3)$ ratios as plotted in these figures.

Considering Figure 4.7, which shows the intensity ratios in samples with a BSF value of 86 %, it can be seen that for all heating times the intensity ratio increased gradually up to a heating temperature of 1200 °C. On moving to heating temperatures higher than 1200 °C, the samples heated for 15 minutes then had a drastic increase in the $I(B_2S):I(BaCO_3)$ ratio. For a heating time of 30 minutes, the ratio also increased markedly on moving from 1300 °C to 1400 °C. For a heating time of 60 minutes, the ratio apparently reached a maximum value at a heating temperature of 1300 °C, after which it decreased again. The samples heated for 120 minutes also appeared to reach a maximum value at a heating temperature of 1300 °C, although the $I(B_2S):I(BaCO_3)$ ratio remained relatively constant from 1200 °C onwards in these samples.

Considering Figure 4.8, it can be seen that in samples with a BSF value of 90 %, the $I(B_2S):I(BaCO_3)$ ratio increased slowly up to a heating time of 1200 to 1300 °C for all heating times. At higher heating temperatures, the $I(B_2S):I(BaCO_3)$ ratio increased much more rapidly. It appears that in samples heated for 15 or 30 minutes, the ratio started to increase at a relatively lower temperature than in the samples that were heated for 60 or 120 minutes.

From Figure 4.9, it can be seen that in samples with a BSF value of 94 %, the $I(B_2S):I(BaCO_3)$ ratio increased gradually up to a heating temperature of 1200 °C, for most heating times. As was the case in samples with the other BSF values, the $I(B_2S):I(BaCO_3)$ ratio then increased rapidly on moving to higher heating temperatures. The only exception to this trend was samples that were heated for 60 minutes. In these samples the ratio increased markedly at temperatures higher

than 1100 °C. The samples that were heated for 120 minutes appeared to reach a maximum value at 1300 °C, after which it decreased again.

In samples with a BSF value of 98 % (Figure 4.10), the $I(B_2S):I(BaCO_3)$ ratio also increased slowly up to a heating temperature of 1200 °C, for most heating times. At heating temperatures higher than 1200 °C the $I(B_2S):I(BaCO_3)$ ratio again increased rapidly for most samples. On moving from a heating temperature of 1300 to 1400 °C, the ratio appeared to level off in samples heated for 30 or 60 minutes. The only exception to this trend was the samples that were heated for 120 minutes. These samples appear to have yielded some irregular results.

Considering Figure 4.11, it can be seen that in samples with a BSF value of 102 %, the $I(B_2S):I(BaCO_3)$ ratio initially increased slowly with heating temperature, for all heating times. On moving from a heating temperature of 1200 °C to higher temperatures, the ratio increased rapidly in samples heated for 15 or 30 minutes. In samples that were heated for 60 or 120 minutes, the ratio increased rapidly when the heating temperature was above 1100 °C. In samples that were heated for 15 minutes, the $I(B_2S):I(BaCO_3)$ ratio continued to increase up to a heating temperature of 1400 °C, while those heated for 30, 60 or 120 minutes reached a maximum value at a temperature of 1300 °C, after which it decreased again.

When considering Figures 4.7 to 4.11, it appears that, irrespective of BSF value, for samples that were heated for 15 to 30 minutes, the ratio of dibarium silicate to barium carbonate increased only very little up to a heating temperature of 1200 °C. On moving to higher heating temperatures, the ratio then increased rapidly in these samples. The samples that were heated for 60 or 120 minutes, in general, appeared to have had sufficient time to react at the lower temperatures for a noticeable increase to occur in the B_2S:BC ratio. Most of these samples showed a significant increase in the B_2S:BC ratio on moving to heating temperatures above 1100 °C. In addition, it seemed that the samples with the highest BSF values, especially the ones that were heated for longest, reached a maximum value for the B_2S:BC ratio at a heating temperature of 1300 °C.

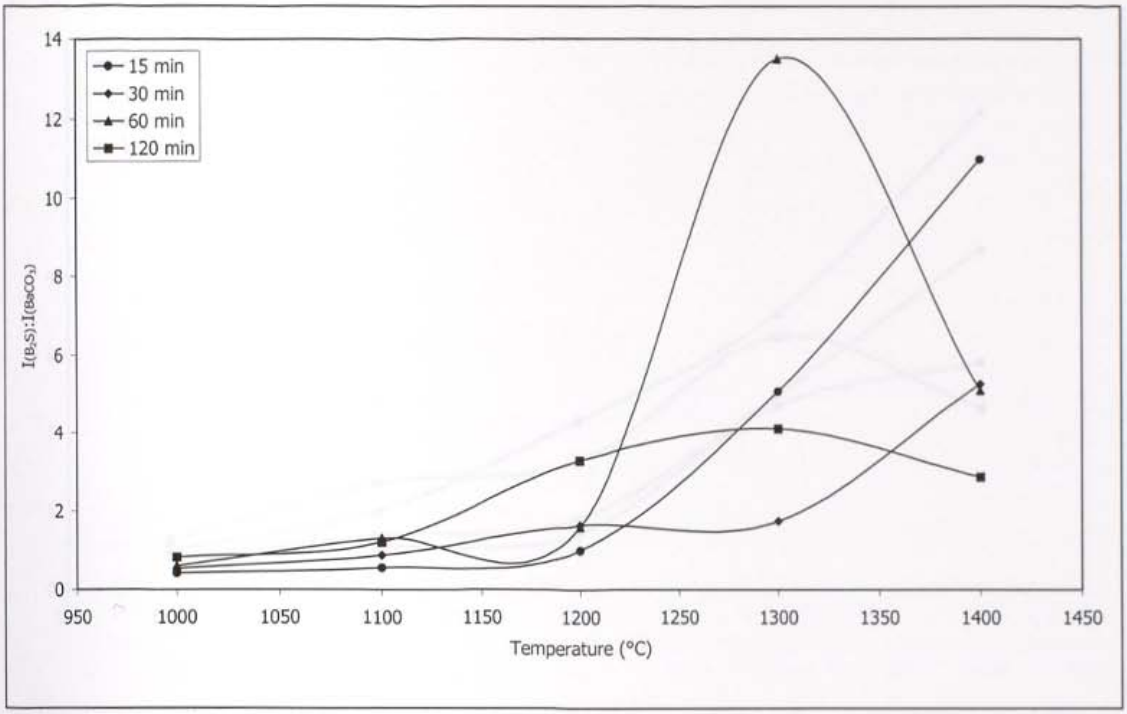

Figure 4.7: Intensity ratio of $B_2S(2\theta = 29.585°):BaCO_3(2\theta = 23.901°)$ with heating temperature for different heating times, for samples with BSF = 86 %

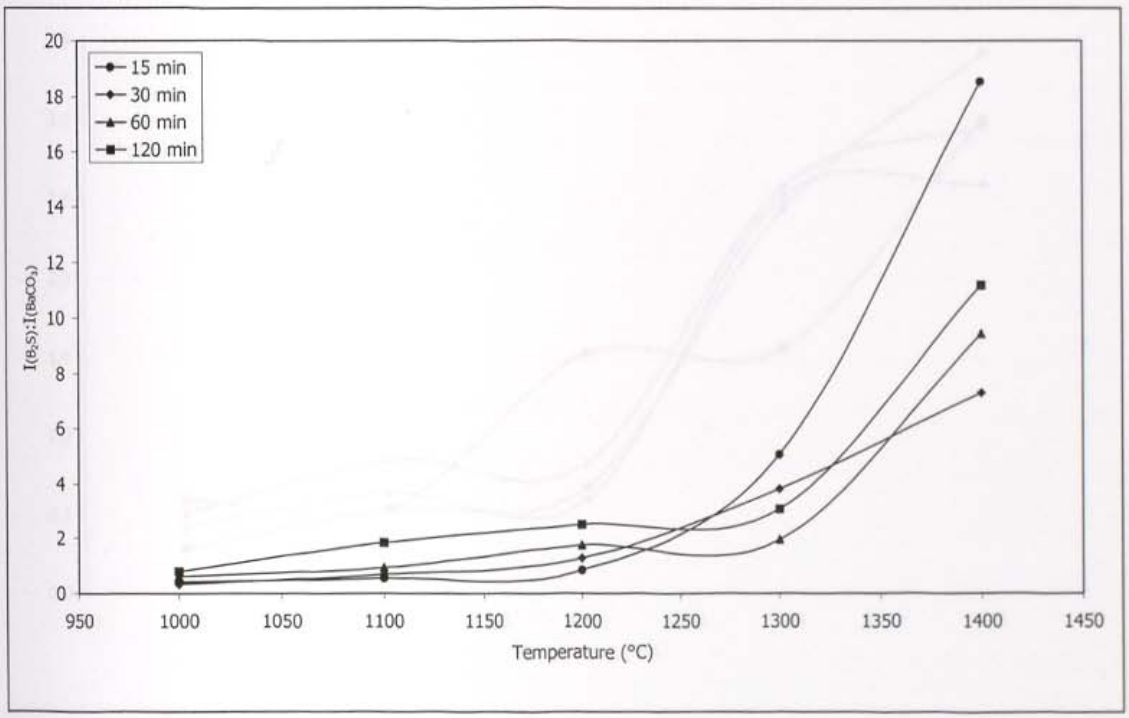

Figure 4.8: Intensity ratio of $B_2S(2\theta = 29.585°):BaCO_3(2\theta = 23.901°)$ with heating temperature for different heating times, for samples with BSF = 90 %

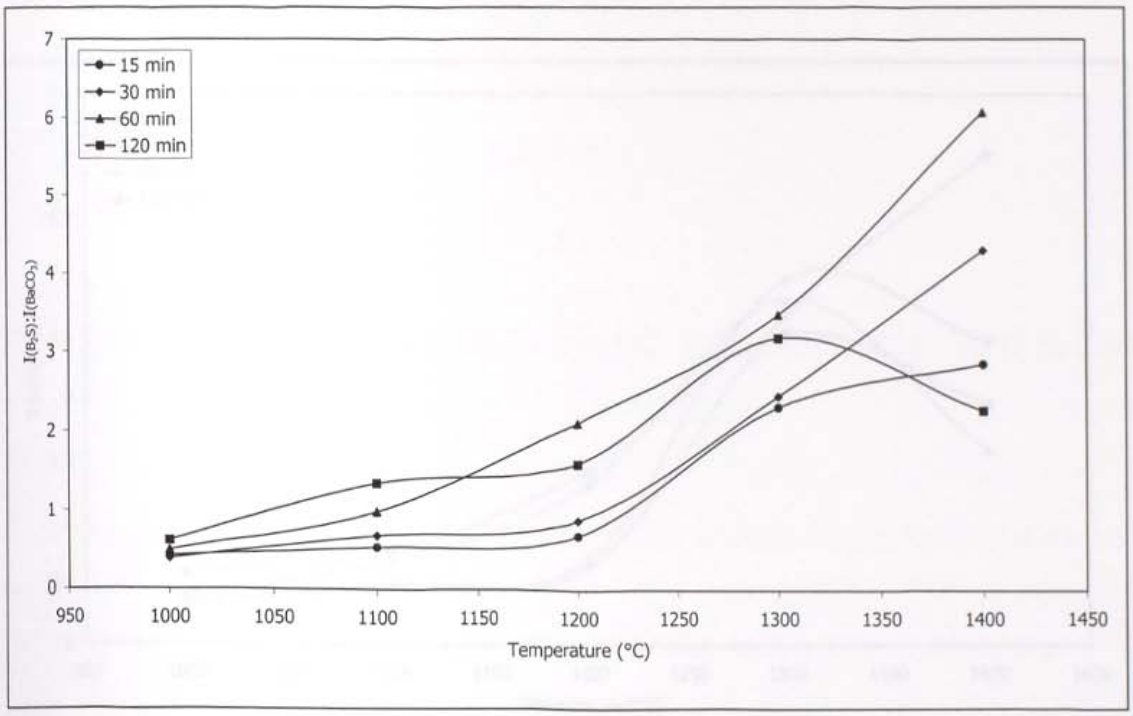

Figure 4.9: Intensity ratio of $B_2S(2\theta = 29.585°):BaCO_3(2\theta = 23.901°)$ with heating temperature for different heating times, for samples with BSF = 94 %

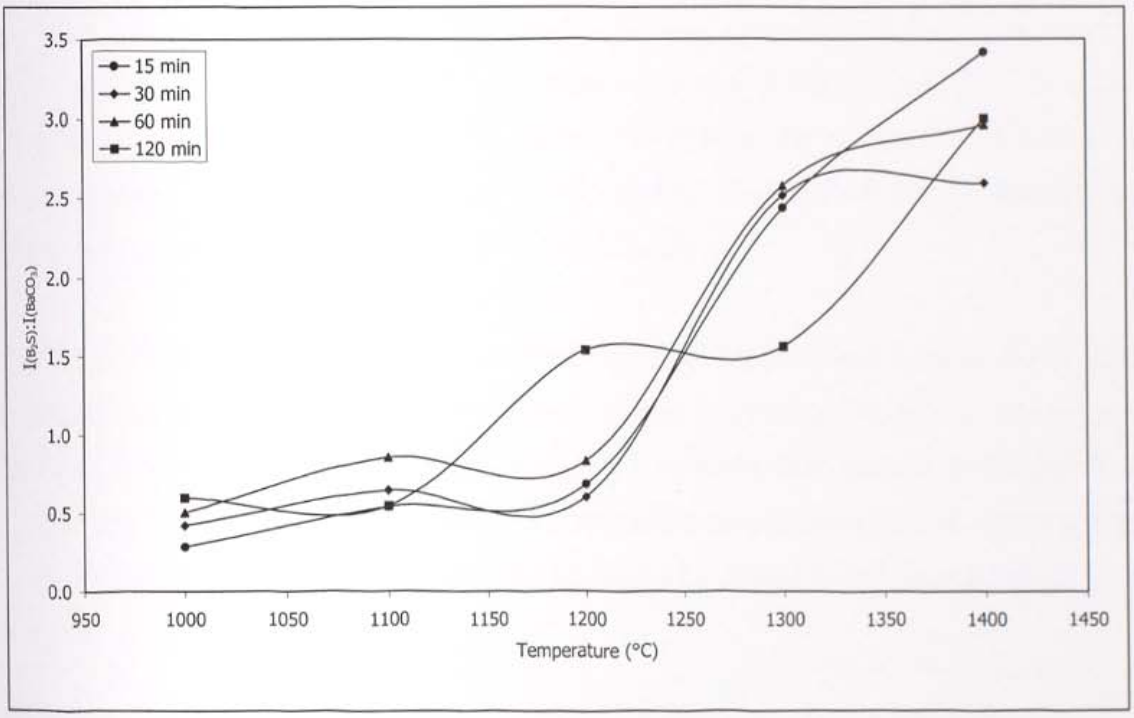

Figure 4.10: Intensity ratio of $B_2S(2\theta = 29.585°):BaCO_3(2\theta = 23.901°)$ with heating temperature for different heating times, for samples with BSF = 98 %

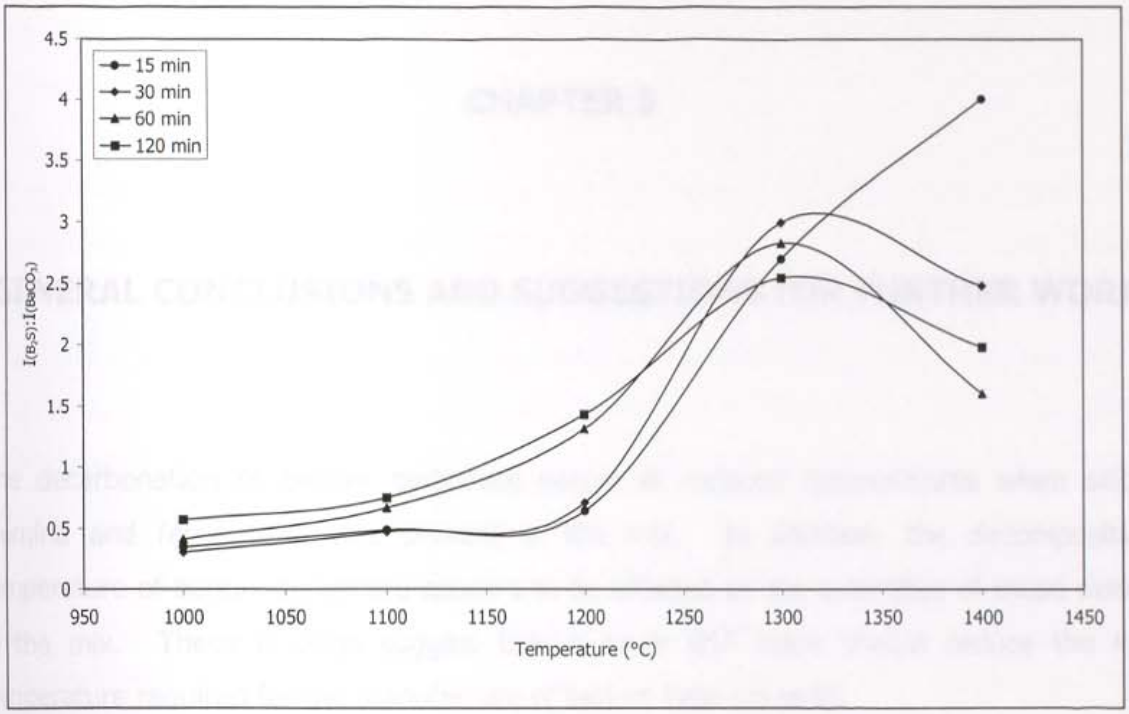

Figure 4.11: Intensity ratio of $B_2S(2\theta = 29.585°):BaCO_3(2\theta = 23.901°)$ with heating temperature for different heating times, for samples with BSF = 102 %